Materials Advances

ROYAL SOCIETY OF CHEMISTRY

PAPER

View Article Online
View Journal | View Issue

Cite this: *Mater. Adv.*, 2022, 3, 7655

Mononuclear nickel(II) complexes as electrocatalysts in hydrogen evolution reactions: effects of alkyl side chain lengths†

Arpita Barma,[a] Malay Chakraborty,[a] Swapan Kumar Bhattacharya, *[a] Pritam Ghosh *[b] and Partha Roy *[a]

Received 25th April 2022,
Accepted 1st August 2022

DOI: 10.1039/d2ma00462c

rsc.li/materials-advances

We report three mononuclear Ni(II) complexes, namely, $[Ni(L^1)_2]$ (**1**), $[Ni(L^2)_2]$ (**2**) and $[Ni(L^3)_2]$ (**3**), where HL^1 = 1-((4-hydroxybutylimino)methyl)naphthalen-2-ol, HL^2 = 1-((5-hydroxypentylimino)methyl)naphthalen-2-ol and HL^3 = 1-((6-hydroxyhexylimino)methyl)naphthalen-2-ol, as electrocatalysts for hydrogen evolution reactions (HERs). Complexes **1**, **2** and **3** were characterized by various standard analytical methods. Single-crystal X-ray structure analysis reveals that nickel is in square planar geometry in all the complexes. These complexes act as efficient electrocatalysts in HERs using acetic acid (AA) and trifluoroacetic acid (TFA) as the proton source in DMF. Controlled-potential electrolysis experiments show that these complexes are capable of reducing protons of AA and TFA to produce H_2. Control experiments show that the complexes are essential for improved production of hydrogen. Theoretical calculations were performed to support the mechanism of HER and to check the effect of chain lengths on the catalytic activity. The catalytic activity runs in the order of complex **1** > **2** > **3**.

Introduction

The need for the development and improvement of secure, sustainable and eco-friendly energy resources is one of the most vital scientific and technical challenges in the present century due to the finite resources of fossil fuels. It is common to use fossil fuel that releases the greenhouse gas, carbon dioxide, into the environment resulting in global warming. In this respect, hydrogen may be considered as a potential candidate for use as an apt energy carrier. The reaction by which molecular hydrogen is produced by two protons *via* the two-electron reduction is known as the hydrogen evolution reaction (HER).[1]

To design an efficient and suitable catalyst for HERs few things such as low price of the metal, metal with labile oxidation states, and coordination sites are to be kept in mind. Platinum has been established as an efficient catalyst for the production of hydrogen.[2] However, it is available in limited quantity and highly expensive. Thus, its extensive use as the catalyst is restricted. Therefore, alternatives are being investigated with much cheaper earth-abundant metals as the catalyst. There are reports of different transition metal complexes[3] with Fe,[4] Mn,[5] Cu,[6] Co[7] and Ni[8] as electrocatalysts for HERs. Various compounds of nickel and cobalt have also been used as the electrocatalysts for water splitting, hydrogen generation, and carbon dioxide reduction, showing their efficient role as electrocatalysts.[9] Due to their inherent better ability towards hydrogen evolution, complexes of cobalt and nickel gain intense interest of researchers as high-performance catalysts.[10] Moreover, Ni(II) systems are abundant in earth,[11] and have relevance to biology.[12] Typically, the hydrogen evolution reaction is operated *via* a metal-centered route, and involves a metal hydride. However, the electrocatalysts consisting of earth-abundant elements are rarely prevailing for HERs under pure aqueous conditions. In most of the cases, organic acids have been used as the substrate in organic media with metal complexes as electrocatalysts.

Nickel(II) complexes with a square planar geometry have been used as catalysts for HERs. Ligands with different donor atoms were designed to get various types of Ni(II) complexes. Generally, NiN_4, NiS_4, NiP_4, NiN_2S_2 and NiS_2O_2 cores have been employed in such catalytic reactions (Scheme 1). Fisher and Eisenberg reported a nickel(II) complex involving a macrocycle with a NiN_4 core as the ligand, as an electrocatalyst for the reduction of carbon dioxide into carbon monoxide and hydrogen as major products.[13] After that, a number of complexes with N_4-donor atoms have been reported in the literature for the same. Mitsopoulou *et al.* reported three Ni(II) diphenyl-1,2-

[a] *Department of Chemistry, Jadavpur University, Kolkata 700 032, India. E-mail: partha.roy@jadavpuruniversity.in, skbhatt7@yahoo.co.in*
[b] *Institut für Chemie, Humboldt-Universität zu Berlin, Brook-Taylor-Straße 2, 12489 Berlin, Germany. E-mail: ppritamghosh@gmail.com*

† Electronic supplementary information (ESI) available. CCDC 2062677 (**1**), 2062678 (**2**) and 2062679 (**3**). For ESI and crystallographic data in CIF or other electronic format see DOI: https://doi.org/10.1039/d2ma00462c

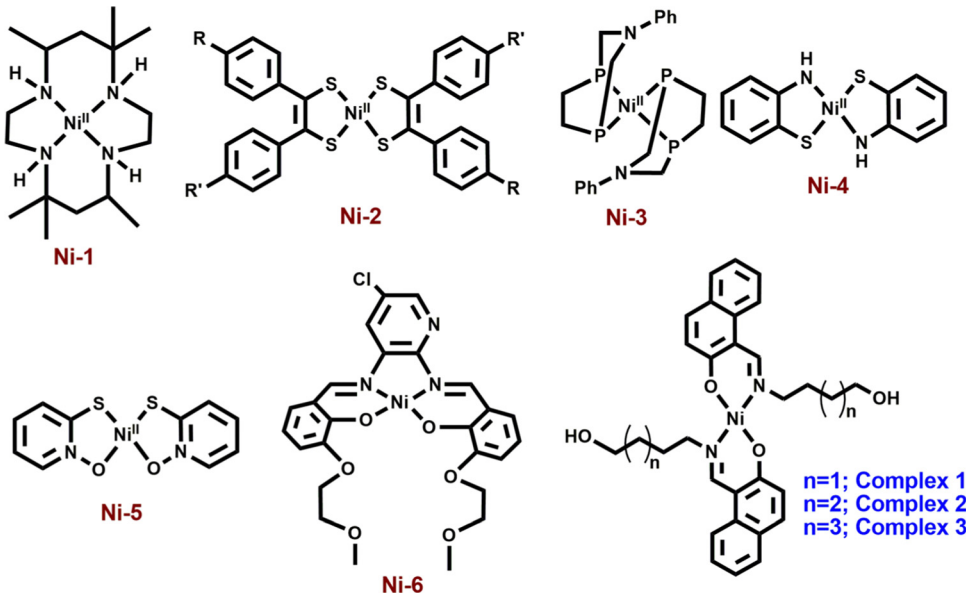

Scheme 1 Different types of mononuclear nickel complexes with NiN_4 (**Ni-1**),[12] NiS_4 (**Ni-2**),[13] NiP_4 (**Ni-3**),[14] NiS_2N_2 (**Ni-4**),[16] NiS_2O_2 (**Ni-5**)[16] and NiN_2O_2 (**Ni-6**)[17] cores for hydrogen evolution reactions.

dithiolene complexes with different substituents on the benzene ring having a NiS_4 core for this purpose and showed the effects of the substituents on the results.[14] Helm and coworkers used a mononuclear nickel(II) complex with two seven-membered cyclic diphosphine ligands having P donor atoms as an highly efficient electrocatalyst for the hydrogen generation.[15] Bergamini and Natali reported a nickel(II) bis(diphosphine) complex as a catalyst for the HER in homogeneous media as well as in heterogeneous media.[16] Eisenberg *et al.* reported a series of nickel complexes with two ligands of N,S or O,S donor sites having square planar coordination for hydrogen evolution with a high turnover number and high stability under conditions of hydrogen production.[17] In comparison to these square planar Ni(II) complexes, very limited number of articles describe the NiN_2O_2 core as the electrocatalyst for hydrogen evolution. Soo *et al.* reported a NiN_2O_2 core as an electrocatalyst for the HER. The presence of alkali metals in the second sphere ether appendages actually increased the hydrogen evolution.[18] The same group has recently reported another nickel complex with a NiO_2N_2 core with different ligand backbones for hydrogen evolution with TONs up to 3880.[19]

Herein, we report the electro-catalytic behavior of three neutral, monomeric Ni(II) complexes, $[Ni(L^1)_2]$ (**1**), $[Ni(L^2)_2]$ (**2**) and $[Ni(L^3)_2]$ (**3**), where HL^1 = 1-((4-hydroxybutylimino)methyl)-naphthalen-2-ol, HL^2 = 1-((5-hydroxypentylimino)methyl)-naphthalen-2-ol and HL^3 = 1-((6-hydroxyhexylimino)methyl) naphthalen-2-ol, for HERs. Complexes **1**, **2** and **3** have been synthesized easily and characterized by several standard methods including single-crystal X-ray diffraction analysis. All of these complexes have been used as electrocatalysts for the reduction of proton in DMF with acetic acid (AA) and trifluoroacetic acid (TFA) as the proton source. Here, we aim to make variation in the ligand chain length of the complexes and to compare the electro-catalytic results obtained under identical conditions. Some theoretical calculations have been performed with insights into the hydrogen evolution mechanism and the effect of chain lengths of ligands on the results.

Experimental section

Materials and physical methods

2-Hydroxy-1-naphthaldehyde, 4-amino-1-butanol, 5-amino-1-pentanol, 6-amino-1-hexanol and nickel(II) perchlorate hexahydrate were purchased from Sigma Aldrich and were used without further purification. Other reagents and solvents were obtained from different commercial sources and used without further purification. Elemental analyses of complexes **1**, **2** and **3** were performed using a Perkin Elmer 2400C elemental analyzer. ^{1}H NMR spectra of three Schiff-base ligands, complexes **1**, **2** and **3**, were recorded using a Bruker 400 MHz spectrometer. FT-IR spectra of complexes **1**, **2** and **3** were recorded using a Perkin Elmer spectrometer (Spectrum Two) with the samples by the ATR method. The UV-visible spectral measurements of complexes **1**, **2** and **3** were performed using an Agilent 8453 diode array spectrophotometer. Cyclic voltammograms were obtained using an electrochemical analyzer (CHI 600C, CH Instruments,) under air-free conditions using a conventional three-electrode cell in which a glassy carbon electrode was used as the working electrode, a saturated Ag/AgCl electrode as the reference electrode, and a platinum wire as the auxiliary electrode. The surface area of the glassy carbon working electrode is 0.07 cm^2. The gas evolved during bulk electrolysis was detected using a GC instrument of model no. 7890B (G3440B), serial no. CN14333203, fitted with TCD. For this, 500 μL gas was taken out in a gas tight syringe from the head space and was injected into the inlet of the GC.

Synthesis of complexes 1, 2 and 3

Synthesis of 1-((4-hydroxybutylimino)methyl)naphthalen-2-ol (HL^1), 1-((5-hydroxypentylimino)methyl)naphthalen-2-ol (HL^2) and 1-((6-hydroxyhexylimino)methyl)naphthalen-2-ol (HL^3). All of the ligands, namely, H_2L^1, H_2L^2 and H_2L^3, were synthesized following a general synthetic procedure. Typically, 0.3 mmol of respective amino alcohol (0.027 g for 4-amino-1-butanol, 0.031 g for 5-amino-1-pentanol and 0.035 g for 6-amino-1-hexanol) was added dropwise into an acetonitrile solution of 2-hydroxy-1-naphthaldehyde (0.3 mmol, 0.0516 g) under stirring. Stirring was continued for further 30 min. The mixture was then refluxed for 4 h when the color of the reaction mixture became yellow. The mixture was then cooled to room temperature. It was filtered to remove solid materials, if any. Solid products were obtained after few days on slow evaporation of acetonitrile.

Data for HL^1: yield = 0.068 g, 92%; anal. calc. (%) for $C_{15}H_{17}NO_2$: C, 74.05; H, 7.04; N, 5.76. Found: C, 73.97; H, 6.96; N, 5.79; ^{1}H NMR (400 MHz, DMSO-d_6, δ ppm, TMS) 14.13 (1H, s), 9.08 (1H, s), 8.07 (1H, d, J = 8.4 Hz), 7.71 (1H, d, J = 9.2 Hz), 7.62 (1H, d, J = 7.6 Hz), 7.42 (1H, m), 7.19 (1H, t, J = 7.2 Hz), 6.72 (1H, d, J = 9.2 Hz), 4.51 (1H, s), 3.66 (2H, t, J = 4.4 Hz), 3.45 (2H, t, J = 4.4 Hz), 1.72 (2H, m), 1.54 (2H, m); ESI-MS$^+$ (m/z): 244.23 [(HL^1 + H^+)].

Data for HL^2: yield = 0.070 g, 90%; anal. calc. (%) for $C_{16}H_{19}NO_2$: C, 74.68; H, 7.44; N, 5.44. Found: C, 74.57; H, 7.36; N, 5.39; ^{1}H NMR (400 MHz, DMSO-d_6, δ ppm, TMS) 14.13 (1H, s), 9.09 (1H, s), 8.06 (1H, d, J = 8.0 Hz), 7.71 (1H, d, J = 9.2 Hz), 7.62 (1H, d, J = 7.6 Hz), 7.42 (1H, t, J = 7.6 Hz), 7.18 (1H, t, J = 7.2 Hz), 6.72 (1H, d, J = 9.2 Hz), 4.33 (1H, s), 3.65 (2H, t, J = 6.8 Hz), 3.42 (2H, t, J = 6.0 Hz), 1.49 (2H, m), 1.29 (2H, m); ESI-MS$^+$ (m/z): 258.11 [(HL^2 + H^+)].

Data for HL^3: yield = 0.069 g, 85%; anal. calc. (%) for $C_{17}H_{21}NO_2$: C, 75.25; H, 7.80; N, 5.16. Found: C, 75.17; H, 7.76; N, 5.29; ^{1}H NMR (400 MHz, DMSO-d_6, δ ppm, TMS) 14.12 (1H, s), 9.08 (1H, s), 8.06 (1H, d, J = 8.4 Hz), 7.70 (1H, d, J = 9.2 Hz), 7.61 (1H, d, J = 8.0 Hz), 7.41 (1H, t, J = 7.2 Hz), 7.18 (1H, t, J = 7.6 Hz), 6.71 (1H, d, J = 9.2 Hz), 4.36 (1H, s), 3.63 (2H, t, J = 7.2 Hz), 3.39 (2H, t, J = 6.0 Hz), 1.67 (2H, m), 1.33 (2H, m); ESI-MS$^+$ (m/z): 272.13 [(HL^3 + H^+)].

Synthesis of [Ni(L^1)] (1). HL^1 (0.6 mmol, 0.146 g) in 5.0 mL of acetonitrile was added slowly into a solution of nickel(II) perchlorate hexahydrate (0.3 mmol, 0.1097 g) in acetonitrile (5.0 mL) under continuous stirring. The mixture was stirred till it turned greenish. Then, it was refluxed for one hour. The color of the solution changed to dark green. The mixture was then cooled to room temperature and filtered to remove solid materials, if any. The filtrate was kept in a beaker under ambient conditions for slow evaporation. Green crystals of complex **1** suitable for single-crystal X-ray diffraction were produced after few days.

Data for **1**: yield, 0.094 g, 58%; anal. calc. for $C_{30}H_{31}NiN_2O_4$: C, 66.45; H, 5.76; N, 5.17; found: C, 66.33; H, 5.80; N, 5.06%. ^{1}H NMR (400 MHz, DMSO-d_6, δ ppm, TMS) 9.11 (1H, s), 8.12 (1H, d, J = 8.4 Hz), 7.83 (1H, d, J = 8.8 Hz), 7.74 (1H, d, J = 8.0 Hz), 7.50 (1H, t, J = 7.6 Hz), 7.25 (1H, t, J = 7.2 Hz), 6.82 (1H, d, J = 8.8 Hz), 4.45 (1H, s), 4.17 (2H, t, J = 5.2 Hz), 3.50 (2H, t, J = 5.6 Hz), 1.97 (2H, m), 1.65 (2H, m).

Synthesis of [Ni(L^2)] (2) and [Ni(L^3)] (3). Complexes **2** and **3** were synthesized following the method used for the synthesis of complex **1**. HL^2 (0.6 mmol, 0.154 g) and HL^3 (0.6 mmol, 0.163 g) were used for complexes **2** and **3**, respectively, in place of HL^1.

Data for **2**: yield, 0.106 g, 62%; anal. calc. for $C_{32}H_{36}NiN_2O_4$: C, 67.27; H, 6.35; N, 4.90; found: C, 67.20; H, 6.26; N, 5.05%. ^{1}H NMR (400 MHz, DMSO-d_6, δ ppm, TMS) 9.15 (1H, s), 8.12 (1H, d, J = 8.8 Hz), 7.85 (1H, d, J = 8.8 Hz), 7.74 (1H, d, J = 8.0 Hz), 7.48 (1H, t, J = 7.6 Hz), 7.27 (1H, t, J = 7.2 Hz), 6.80 (1H, d, J = 8.8 Hz), 4.35 (1H, s), 4.24 (2H, t, J = 5.2 Hz), 3.43 (2H, t, J = 5.2 Hz), 1.94 (2H, m), 1.52 (2H, m).

Data for **3**: yield, 0.104 g, 58%; anal. calc. for $C_{34}H_{40}NiN_2O_4$: C, 68.13; H, 6.73; N, 4.67; found: C, 68.05; H, 6.80; N, 4.58%. ^{1}H NMR (400 MHz, DMSO-d_6, δ ppm, TMS) 9.12 (1H, s), 8.11 (1H, d, J = 8.0 Hz), 7.89 (1H, d, J = 8.8 Hz), 7.74 (1H, d, J = 7.2 Hz), 7.50 (1H, t, J = 7.2 Hz), 7.25 (1H, t, J = 8.0 Hz), 6.79 (1H, d, J = 8.8 Hz), 4.32 (1H, s), 3.38 (2H, t, J = 5.2 Hz), 3.33 (2H, t, J = 6.4 Hz), 2.29 (2H, m), 1.48 (2H, m).

CAUTION: nickel(II) perchlorate hexahydrate can be explosive on heating. Therefore, the perchlorate salts should be handled with care.

X-ray data collection and structure determination

Data collection and refinement parameters for complexes **1**, **2** and **3** are summarized in Table 1. The X-ray diffraction experiments were performed using a BRUKER D8 QUEST CCD diffractometer for **1** and a Bruker APEX-II CCD diffractometer for **2** and **3** with graphite-monochromated Mo Kα radiation at 294(2) K. Data processing was done using the Bruker *APEX2* and *SAINT* packages.[20] Absorption corrections, which are based on multi-scans using the *SADABS* software,[20] were applied to intensity data. The structures of complexes **1**, **2** and **3** were solved by direct methods utilizing SHELXT[21] and refined with full-matrix least-squares on F^2 on all unique reflections employing SHELXL-2014/7.[22] All the non-hydrogen atoms of all of three complexes were refined anisotropically. The crystals selected for the single-crystal X-ray diffraction analysis of complexes **1** and **3** were refined as merohedral twins in both the complexes with a fractional contribution of minor components of 0.18(3) and 0.03(2), respectively. In complex **1**, the quality of crystal was poor. The poor quality as well as the presence of twinning in **1** may account for the limited overall precision of its structure, high residual peaks and the relatively high values of R and wR_2 parameters.

CCDC 2062677, 2062678 and 2062679 contain the supplementary crystallographic data for complexes **1**, **2** and **3**, respectively.†

Results and discussion

Synthesis of ligands and their characterization by ESI mass and ^{1}H spectral analysis

1-((4-Hydroxybutylimino)methyl)naphthalen-2-ol (HL^1), 1-((5-hydroxypentylimino)methyl)naphthalen-2-ol (HL^2) and 1-((6-hydroxyhexylimino)methyl)naphthalen-2-ol (HL^3) were synthesized by a Schiff-base condensation reaction between 2-hydroxy-1-naphthaldehyde and the respective amine in 1 : 1 proportion in

Table 1 Crystal data of complexes **1**, **2** and **3**

Complex	**1**	**2**	**3**
Formula	$C_{30}H_{31}N_2Ni_1O_4$	$C_{32}H_{36}N_2$ Ni_1O_4	$C_{34}H_{40}N_2$ Ni_1O_4
Formula weight	542.26	571.32	599.39
T (K)	298(2)	298(2)	298(2)
Crystal color	Green	Green	Green
Crystal system	Monoclinic	Triclinic	Triclinic
Space group	$P21/c$	$P\bar{1}$	$P\bar{1}$
a (Å)	10.7840(8)	4.9186(4)	5.1838(7)
b (Å)	4.9890(4)	16.7080(14)	16.905(2)
c (Å)	23.8099(18)	16.9064(14)	17.141(2)
α (°)	90	86.436(3)	84.192(5)
β (°)	90.846(2)	84.966(2)	87.843(4)
γ (°)	90	89.509(2)	89.703(4)
V (Å^3)	1280.87(17)	1381.3(2)	1493.3(3)
Z	2	2	2
Crystal dimensions (mm)	0.40 × 0.26 × 0.13	0.41 × 0.23 × 0.12	0.46 × 0.29 × 0.16
F(0 0 0)	570.0	604.0	636.0
D_c (g cm^{-3})	1.406	1.374	1.333
λ(Mo Kα) (Å)	0.71073	0.71073	0.71073
θ range (°)	2.53–27.11	2.65–27.25	2.39–27.00
Reflection collected/unique/observed	29 207, 2837, 2507	70 198, 6202, 5565	78 729, 6626, 5259
Absorption correction	Multi-scan	Multi-scan	Multi-scan
R_{int}	0.0306	0.0320	0.0350
Final R_1 index [$I > 2\sigma(I)$]	0.0352	0.0348	0.0498
Final wR_2 index (all reflections)	0.1324	0.1024	0.1397
Goodness-of-fit	1.166	1.022	0.925

acetonitrile with high yields (Scheme S1, ESI†). Complexes **1**, **2** and **3** were obtained by the reactions between the ligands and nickel(II) perchlorate hexahydrate in 2 : 1 proportion without the addition of any external base.

ESI-mass spectrometric measurements of HL^1, HL^2 and HL^3 were performed with their methanolic solutions (Fig. S1–S3, ESI†). Mass spectrum of HL^1 shows an m/z peak at 244.23, which may be attributed to the $[HL^1 + H^+]$ species (calculated value 244.31). The m/z peak at 258.11 may be assigned to the presence of $[HL^2 + H^+]$ species (calculated value 258.15). The mass spectrum of HL^3 shows an m/z peak at 272.13, which may be due to the presence of $[HL^3 + H^+]$ (calculated value 272.17). These ligands were further characterized by ^{1}H NMR spectral studies (Fig. S4–S6, ESI†). Spectra were obtained in DMSO-d_6. NMR spectral studies support the formation of Schiff-base ligands. All of these compounds show a peak at around 14.1 ppm, which indicates the presence of a phenolic OH group. The peak at around 9.0 ppm in all the ligands may be due to the presence of an imine proton, indicating the formation of Schiff-base compounds. Signals for aromatic protons for all of the ligands appear in the appropriate positions. Signals for methylene protons also appear in their usual positions. All of these analyses support formation of the Schiff-base ligands.

Characterization of complexes 1, 2 and 3

Crystal structures of complexes 1, 2 and 3. Single crystals of complexes **1**, **2** and **3** were obtained on slow evaporation of their acetonitrile solution. Complex **1** crystallizes in a monoclinic system and a $P21/c$ space group. However, both complexes **2** and **3** crystallize in a triclinic system and $P\bar{1}$ space group. The asymmetric unit consists of one nickel centre and a pair of ligands for all of the complexes (Fig. 1). All of **1**, **2** and **3** are mononuclear complexes (Fig. S7–S9, ESI†). The selected bond lengths and bond angles are listed in Table S1 (ESI†). All of these complexes may be summarized as the NiO_2N_2 core. For all of the complexes, the Ni atom is coordinated to N and O donor atoms from a ligand and another set of N and O donor

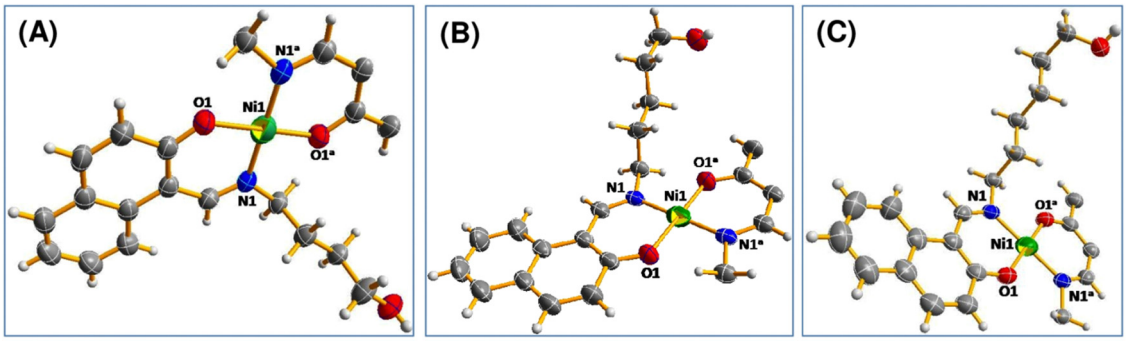

Fig. 1 Perspective view of (A) complex **1**, (B) complex **2** and (C) complex **3** with displacement ellipsoids drawn at the 50% probability level.

atoms from a different ligand. Ni atom is in a square planar geometry. Apart from the hydroxyl alkyl chain, the rest of the molecule is planar. For complex **1**, angles O1–Ni1–O1[a] and N1–Ni1–N1[a] are 180°, whereas other donor–metal–donor angles range from 87.86 to 92.14°. While other donor–metal–donor angles vary from 87.82 to 92.18° for complex **2**, they vary from 88.44 to 91.56° for complex **3**.

For other two complexes, all of the large donor–metal–donor angles are 180°. For a four-coordinate complex, Houser and co-workers proposed the four-coordinate τ_4 index to ascertain the geometry around the metal center. The four-coordinate τ_4 index value was obtained using the following formula:[23]

$$\tau_4 = \frac{360^\circ - (\alpha + \beta)}{141^\circ}$$

where α and β are the two largest donor–metal–donor angles in a tetra-coordinated complex. For a tetrahedral geometry, the value of τ_4 is 1.00, while for an ideal square planar arrangement, it is 0.00. As two largest donor–metal–donor angles are 180° for all of these three complexes, the values of four-coordinate τ_4 index come out as 0.00 for all the complexes. This fact indicates that there exists the perfect square planar geometry around the nickel atom in complexes **1**, **2** and **3**. The O–Ni bond distances are close to 1.82 Å and the O–Ni bond distances are about 1.91 Å. These values are in agreement with the published results.[24]

ESI-mass, FT-IR, UV-vis and ^{1}H NMR spectral characterization of the complexes

ESI-mass spectra of complexes **1**, **2** and **3** were obtained with their methanolic solutions (Fig. S10–S12, ESI†). All of them behave similarly. The mass spectrum of **1** exhibits an *m*/*z* peak at 565.0727, which may be attributed to the $[Ni(L^1)_2 + Na^+]$ species (calculated value = 565.16). This indicates that the complex exists mainly as a mononuclear nickel(II) species in solution. For complex **2**, an *m*/*z* peak appears at 593.10, which may be assigned to $[Ni(L^2)_2 + Na^+]$ (calculated value = 565.19). Similarly, the *m*/*z* peak at 621.14 of complex **3** appears due to the presence of $[Ni(L^3)_2 + Na^+]$ species (calculated value = 621.22).[25]

FT-IR spectra of complexes **1**, **2** and **3** were recorded with a solid sample by the ATR technique (Fig. S13–S15, ESI†). In the IR spectra, broad bands appear at 3536 cm^{-1}, 3316 cm^{-1} and 3272 cm^{-1} for complexes **1**, **2** and **3**, respectively. The peaks were assigned to O–H stretching for the presence of a hydroxyl group in the ligand part of the complexes. The presence of a methylene group in the complexes has been evidenced by the appearance of unsymmetrical and symmetrical frequencies of ν_{C-H} in the range of 2800–3000 cm^{-1}. In the IR spectra of complexes **1**, **2** and **3**, intense bands appeared at ~1657 cm^{-1}, 1658 cm^{-1} and 1642 cm^{-1} respectively. These may be attributed to the presence of the C=N moiety in the complexes. The conclusive evidence for the formation of Ni–N and Ni–O bonds in the IR spectra of these complexes is also observed with characteristic bands. These bands support the fact that the metal ion has been effectively coordinated to the four coordinating heteroatoms (NONO). These data are also supported by the literature (Table S2, ESI†).[26]

The UV-vis spectra of complexes **1**, **2** and **3** were recorded in the range of 200–800 nm in DMF at room temperature (Fig. S16–S18, ESI†). The electronic spectra of these complexes are grossly similar in nature. A broad band at around 600 nm was observed for each of the complexes, which may be attributed to the *d*–*d* transition. These are weak in intensity as they are Laporte forbidden.[27] The bands at 275 nm for complex **1**, 279 nm for complex **2** and 274 nm for complex **3** may be assigned to the π–π* transitions of the phenolic chromophore. The bands between 300 and 500 nm may be assigned to the π–π* transition of the azomethine chromophore and the benzene ring and the n–π* transition of the azomethine chromophore.[28] The higher intensity charge-transfer transition has been observed at a wavelength near 420 nm for all three complexes. These are attributed to O^- (of naphthalen-1-olate) → Ni(II), N(amino) → Ni(II) LMCT and intra-ligand charge transfer transitions.[29] All of these bands corroborate the structure of the complexes (Table S3, ESI†).

^{1}H NMR spectra of complexes **1**, **2** and **3** were obtained in DMSO-d_6 (Fig. S19–S21, ESI†). The behavior of all the ligands in the presence of Ni^{2+} is grossly similar. All of these complexes are square planar in geometry and the metal ion in the complex does not possess any unpaired electron. The peak for phenolic OH at ~14 ppm is absent in the NMR spectra of all the complexes. This indicates that the phenolic OH group is deprotonated during complex formation and then coordinated to the metal center. The signal for the imine proton at ~8 ppm in the ligands undergoes a shift to ~9 ppm for all the complexes, confirming complex formation *via* azomethine nitrogen atoms. Signals for aromatic protons shift towards higher δ values. All other peaks appear in their usual positions. The fact indicates that all of the complexes remain the same in the DMSO solution.[25]

Electrochemistry

Cyclic voltammetric studies. As shown in Fig. 2(A)–(C), cyclic voltammograms of complexes **1**, **2** and **3** respectively were recorded in air-free DMF containing 0.1 M tetrabutylammonium bromide in the range of −2 V to +2 V *versus* Fc/Fc^+. An important feature of these cyclic voltammograms is the nickel(II)–nickel(I) redox couple with cathodic peak potentials (E_{pc}) of −1.48, −1.51, −1.52 V *versus* Fc/Fc^+ for complexes **1**, **2** and **3** respectively, while anodic peak potentials (E_{pa}) of −0.77, −0.68 and −0.74 V *versus* Fc/Fc^+ for complexes **1**, **2** and **3** respectively.[30] Considering the reduction sweep, initially, an irreversible event is observed at −0.85, −0.76 and −0.73 V *versus* Fc/Fc^+ for complexes **1**, **2** and **3** respectively due to the electrochemically irreversible Ni(III)/Ni(II) reductive response,[31] while another quasi reversible redox event observed for each of the complexes at 0.5 V *versus* Fc/Fc^+ appears for the solvent DMF. The nature of the voltammograms of the complexes scanned over the presently important region of potential of reversible Ni(II/I) couple (−2 V *versus* Fc/Fc^+ to +0.6 V *versus* Fc/Fc^+) is shown in the insets of Fig. 2. In Fig. 2(D), the cyclic voltammogram of ferrocene is presented in the DMF

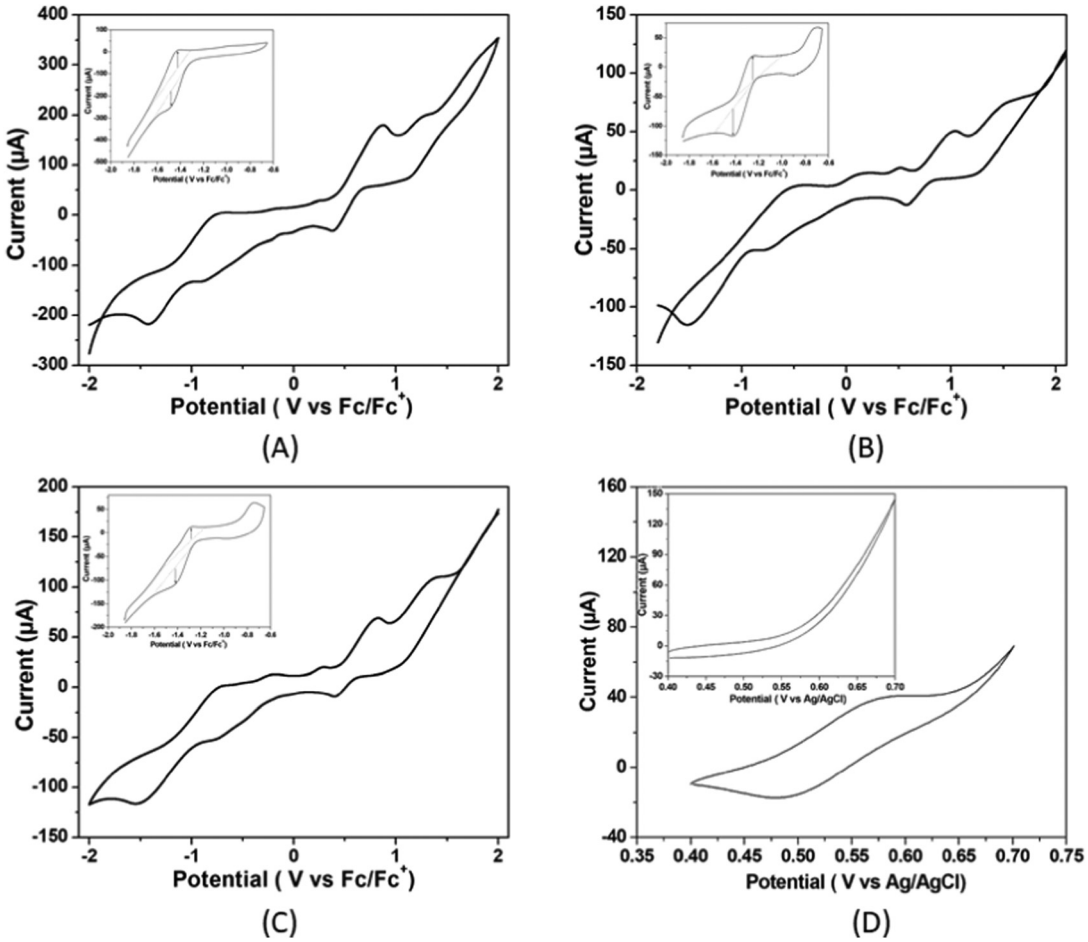

Fig. 2 Cyclic voltammograms of 5.36 μM of (A) complex **1**, (B) complex **2** (C) complex **3** and (D) ferrocene (inset: cyclic voltammograms scanned over the presently important region of potential of reversible Ni(II/I) couple) in air free DMF solutions with 0.1 M of [*n*-Bu_4N]Br as the supporting electrolyte at a scan rate of 50 mV s^{-1}. Here, ferrocene is the internal standard.

solution on the same working electrode. The $E_{1/2}$ value obtained (0.535 V *versus* aqueous AgCl/Ag, Cl^- electrode or 0.559 V *versus* NHE) is very close to the value reported in the literature.[32]

The current responses of the redox events at −1.48, −1.51, and −1.52 V *versus* Fc/Fc^+ for complexes **1**, **2** and **3** respectively at multiple scan rates from 0.02 to 0.15 V s^{-1} were used to construct the Cottrell plot. The plots show linear dependence of the current response on the square root of the scan rate (Fig. S22, ESI†). This indicates that for the three complexes, the reduction is diffusion limited with a diffusion coefficient of 1.07×10^{-5} for complex **1**, 0.77×10^{-5} for complex **2** and 0.72×10^{-5} for complex **3** (please see ESI†). It has been observed that the catalytic-to-peak current ratio (i_{cat}/i_p) increases for all the three complexes with the increase in acid concentration (Fig. S23, ESI†).

The electrochemical properties of three nickel(II) complexes with salen-type ligands were influenced by the presence of different substituents of the imine linkage.[33] Ren and co-workers showed that the electrochemical reduction ability of nickel(II) complexes with cyclam ligands from H^+ to H_2 is dependent on the substituents of the macrocyclic ligands.[34] Thus, it is expected that changes in the chain length of ligands in the Ni(II) complexes in the present study could influence Ni(II)/Ni(I) potentials of the complexes.

Electrocatalytic hydrogen evolution in DMF: CV studies. The performance of these three mononuclear Ni(II) complexes as effective electrocatalysts for the HER was assessed under various conditions, in which the proton source (CH_3COOH or CF_3COOH) has been systematically varied.

To determine the activity of complexes **1**, **2** and **3** as electrocatalysts, first, cyclic voltammograms of the complexes were recorded in the presence of acetic acid (pK_a = 13.5) in DMF.[35] The addition of CH_3COOH aliquots at a concentration ranging from 0.00 to 24.00 mM to the solutions of complexes **1**, **2** and **3** in DMF triggers the systematic increase in catalytic current (i_{cat}) at −1.48, −1.51, and −1.52 V respectively *versus* Fc/Fc^+ (Fig. 3).

The onset potentials for the reduction of hydrogen ions in the presence of the three complexes studied are −1.13 V, −1.15 V and −1.20 V *versus* Fc/Fc^+, respectively, indicating that the catalytic activity is in the order: complex **1** > complex **2** > complex **3**.

The electrocatalytic activity of these complexes was also accessed using trifluoroacetic acid (pK_a = 6.0) in DMF as a proton source.[36] As shown in Fig. 4, there is an increase in the

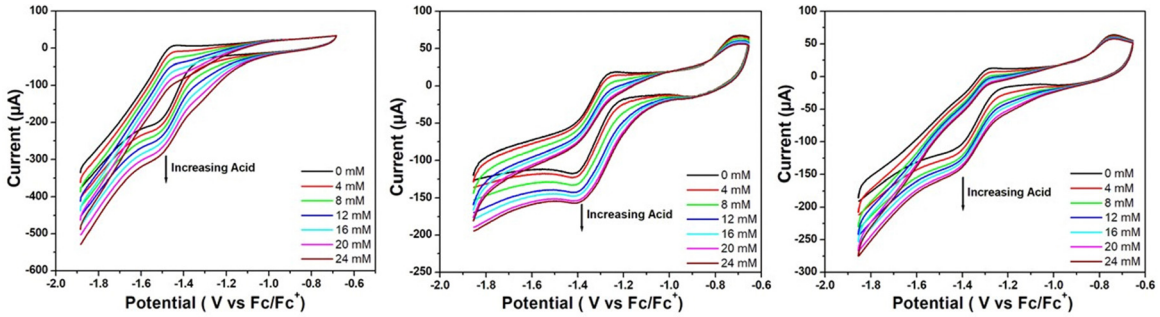

Fig. 3 Cyclic voltammograms of (A) complex **1**, (B) complex **2** and (C) complex **3** (5.36 μM) in the absence of acetic acid (black trace) and in the presence of different concentrations of acetic acid in air-free DMF. Conditions: 25 °C, 0.1 M [*n*-Bu_4N]Br as the supporting electrolyte, scan rate = 50 mV s^{-1}, glassy carbon working electrode, Pt wire counter electrode and the potential are referenced against Fc/Fc^+.

catalytic current (i_{cat}) at −1.48, −1.51, and −1.52 V *versus* Fc/Fc^+ for complexes **1**, **2** and **3** respectively upon successive addition of CF_3COOH (0.00 to 24.00 mM). For all the three complexes, the peak current increases and the peak potential is shifted towards less negative potential (anodically) with the increase in acid concentration in the solution. This signifies that the greater diffusion of proton from bulk solution to the electrode surface makes the reduction process much easier at high concentrations of acid. Notably, for all the three complexes, the sequence of peak currents that also represents their catalytic activity at any particular acid concentration is the same as the order of post peak current values, which decrease sharply with the decrease in potential due to increased hydrogen evolution.

This rise in current in both the cases could be attributed to the generation of H_2 from catalytic reduction of protons. The reduction potentials of these complexes slightly change towards more anodic values with the sequential enhancements in the concentration of the acid. The overpotential for hydrogen evolution was calculated following the methods reported by Fourmond *et al.*[35] from the theoretical half wave potential, $E^{T}_{1/2}$, based on the expression found in the supporting document and the experimental potential $E_{cat/2}$ (eqn (1)):

$$\text{Over potential } (\eta) = |E^{T}_{1/2} - E_{cat/2}| \quad (1)$$

Based on eqn (1), this reduction occurs at overpotentials of −0.52 V, −0.55 V and −0.56 V for complexes **1**, **2** and **3** respectively for the former case, where acetic acid is the proton source. The corresponding values are −0.22 V, −0.23 V and −0.24 V for complexes **1**, **2** and **3** respectively for the latter case, where trifluoroacetic acid is the proton source.

In both the cases, the catalytic activity of the three homogeneous catalysts as obtained from the overpotential value is in the following order: complex **1** > complex **2** > complex **3**. Moreover, the large difference in overpotential for each complex for the two proton sources is expected for the increased diffusion of protons in the latter case.

A table is given in ESI† (Table S4), where few of recently reported Ni(II) complexes[8b,c,37] are listed with their overpotential values. In most of the cases, the medium of experiment was organic. The proton source varies as acetic acid, trifluoroacetic acid, perchloric acid or buffer solution. If we look into the values of overpotential, they are in the range of few millivolts. While comparing with the other reported overpotential values for the electrocatalytic hydrogen evolution catalysed by nickel complexes as enlisted in the table, it can be concluded that these three nickel(II) complexes are more effective in this field.

The stability of all three complexes have been checked by repeated cyclic voltammetry (CV) studies up to 65 cycles using

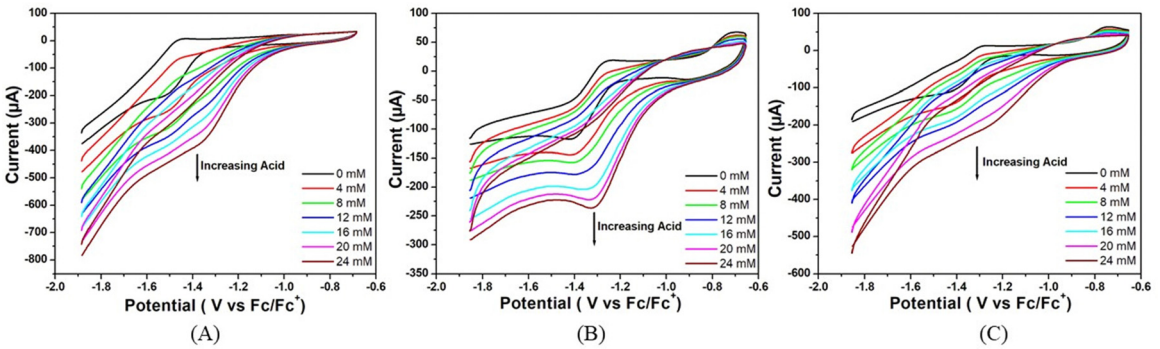

Fig. 4 Cyclic voltammograms of (A) complex **1**, (B) complex **2** and (C) complex **3** (5.36 μM) in the absence of trifluoroacetic acid (black trace) and in the presence of different concentrations of trifluoroacetic acid in air-free DMF. Conditions: 25 °C, 0.1 M [*n*-Bu_4N]Br as supporting electrolyte, scan rate = 50 mV s^{-1}, glassy carbon working electrode, Pt wire counter electrode and the potential is referenced against Fc/Fc^+.

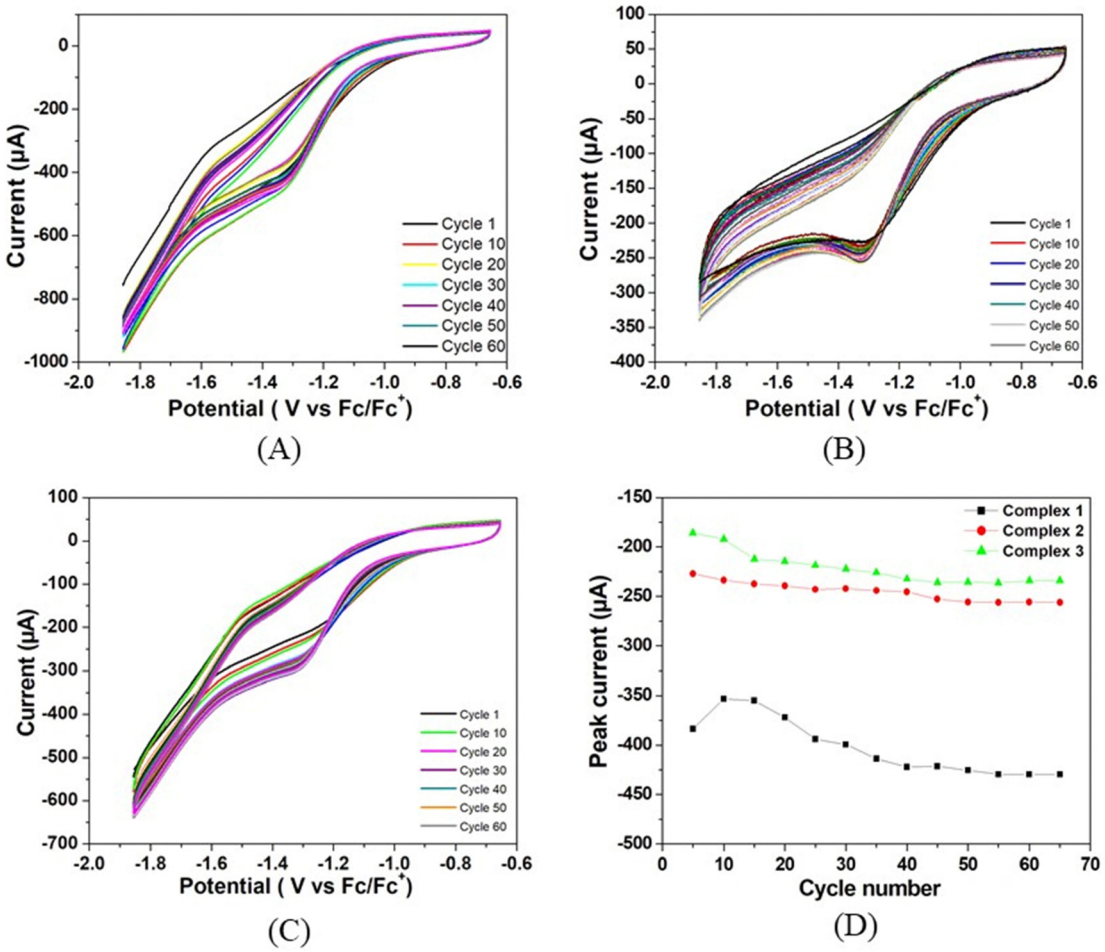

Fig. 5 Repeated cyclic voltammetry studies of (A) complex **1**, (B) complex **2**, and (C) complex **3**. (D) Peak current *vs.* cycle number profiles for all the three complexes.

TFA as the proton source (Fig. 5). It has been observed that no new peaks are generated in the CV and also the colour of the solution remains the same during the study. In all cases, the reduction peak current increases continuously and reaches almost a steady value at the 55th cycle. The peak current with respect to the lowest amount is increased by 12% for complex **1**, 14% for complex **2**, and 28% for complex **3**. The current of complex **1** is always greater than the remaining two complexes. The increase in current during repeated cyclic voltammetric operation might be due to the cleansing of the fine surface of the electrode and opening up of new channels by the initial H^+ ion penetration at the metal centre and the associated H_2 evolution. Thus, more active sites of the electrode surface are created for further reaction. Greater the size of the alkyl group, the greater is the initial prevention of H^+ for approaching towards the metal centre for reduction. On application of the negative potential, the proton penetrates through the barrier and creates new channels for further reaction. Since the initial barrier varies in the order of complex **3** > complex **2** > complex **1**, the increase in the peak current on cycling is in the reverse order.

Electrocatalytic hydrogen evolution: CPE studies. Further evidence for the electrocatalytic activity of these mononuclear nickel(II) complexes for HERs was evaluated in DMF by conducting controlled-potential electrolysis (CPE) experiments over a period of 1 h, as in Fig. 6, 7 and Table 2. Fig. 6 shows the total charge of bulk electrolysis of 5.36 μM of complex **1**, **2** and **3** separately in DMF solutions in the presence of acetic acid (24 mM). At an applied potential of −1.5 V *versus* Fc/Fc^+, the maximum charge reached during 1 hour of electrolysis is 0.73 C for complex **1**, 0.51 C for complex **2** and 0.44 C for complex **3**, accompanied by gas bubbles appearing on the electrode (Fig. S24, ESI†).

However, when the CPE experiments were done with 5.36 μM of complexes **1**, **2** and **3** separately in DMF solutions in the presence of trifluoroacetic acid (24 mM), the same trend was obtained (Fig. 7). At an applied potential of −1.50 V *versus* Fc/Fc^+, the maximum charge reached 1.41 C for complex **1**, 0.61 C for complex **2** and 0.49 C for complex **3** during 1 hour of electrolysis. CPE experiments under the same potential with a catalyst-free solution gave only a charge of 0.11 C, showing that complex **1** is again more effective than the remaining two complexes in hydrogen production under such conditions. This study suggests that all these three complexes are capable of catalysing the reduction of protons from acid to H_2. The

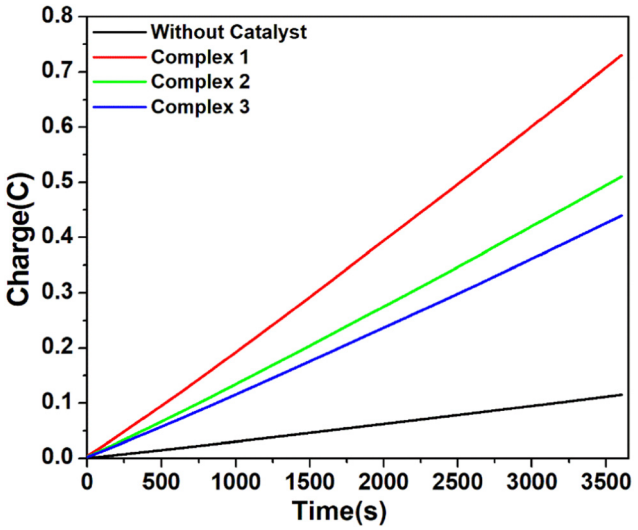

Fig. 6 Charge build up *vs.* time plots in the CPE (controlled potential electrolysis) experiment of complex **1** (red), complex **2** (green), and complex **3** (blue) and without catalyst (black) at potential −1.5 V *versus* Fc/Fc^+. Conditions: 5.36 μM complex in air-free DMF with 0.1 M [*n*-Bu_4N]Br as the supporting electrolyte and 24 mM CH_3COOH as the proton source.

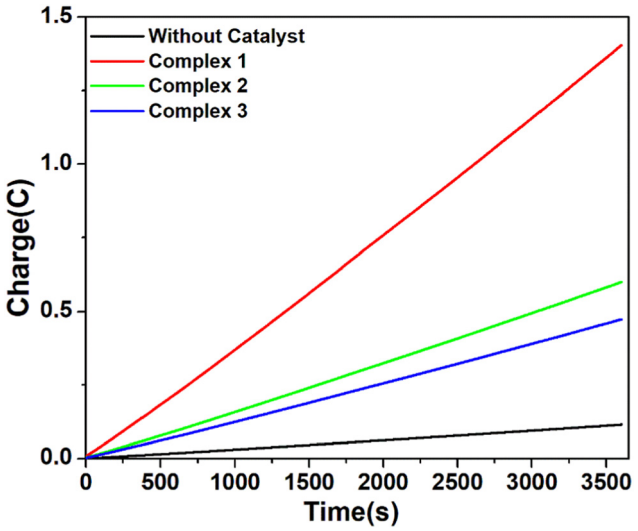

Fig. 7 Charge build up *vs.* time plots in the CPE (controlled potential electrolysis) experiment of complex **1** (red), complex **2** (green), and complex **3** (blue) and without catalyst (black) at potential −1.5 V *versus* Fc/Fc^+. Conditions: 5.36 μM complex in air-free DMF with 0.1 M[*n*-Bu_4N]Br as the supporting electrolyte and 24 mM CF_3COOH as the proton source.

evolution of H_2 gas has been confirmed by the use of gas chromatography (Fig. S25, ESI†). The turn over number (TON) and faradaic efficiency were calculated for all the complexes (Tables S5 and S6, ESI†), and the result of CPE experiments is enlisted in Table 2.

The turnover frequency (TOF) for hydrogen evolution using all the three complexes **1**, **2** and **3** as electrocatalysts was estimated by the foot-of-the-wave analysis (FOWA).[38] The FOWA has been considered near the foot of the catalytic wave, where the catalytic wave does not get affected much by phenomena such as substrate consumption, diffusion and shape of CV dominated mainly by catalytic phenomenon.[39] The i_{cat}/i_p was plotted against $1/(1 + \exp[(F/RT)(E - E_{1/2})])$ for both the complexes, as given in Fig. S26 and S27 (ESI†), and the obtained TOF values are presented in Table S5 (ESI†).

Table 2 Results of CPE experiments with complexes **1**, **2** and **3**

Complex	Solvent	Proton source	*q* (C)	*n* ($\times 10^{-6}$)	TON	TOF (s^{-1})	Faradaic efficiency (%)
1	DMF	Acetic acid	0.62	3.21	23.95	251.25	67.56
2			0.40	2.07	15.45	133.75	48.64
3			0.33	1.71	12.76	92.92	41.35
1		Trifluoroacetic	1.30	6.74	50.30	426.67	81.78
2		acid	0.50	2.59	19.33	188.75	61.41
3			0.38	1.97	14.70	126.67	59.58

Determination of the reaction mechanism of HERs by the Tafel analysis. The Tafel analysis is generally employed to understand the catalytic kinetics of hydrogen evolution reactions (Fig. 8). The Tafel slope is regarded as an inherent property of electrocatalyst and is evaluated by the rate limiting step for HERs. Its analysis is vital for enlightening the mechanism of the HER. According to the Tafel equation,

$$\eta = a + b \log i \quad (2)$$

where η = overpotential, a = constant, b = Tafel slope and i = measured current density.

A low η value corresponds to a large exchange current density (i_0, current density at $\eta = 0$), whereas a low b value indicates better hydrogen evolution and hence a better catalytic activity.[40] In this case, the determined Tafel slopes for complex **1** are 1.81 V dec^{-1} and 1.86 V dec^{-1} for the acid sources trifluoroacetic acid and acetic acid, respectively indicating that trifluoroacetic acid will lead to a faster increase in reaction rate (fast proton discharge kinetics on the working electrode) with the increase in potential.

Electrocatalytic hydrogen evolution: control experiments. To confirm the role of these three nickel complexes in HERs and to ascertain the hydrogen evolution not due to the complex adsorbed on the surface or degradation products of the complex, different control experiments were conducted. First, blank CVs were recorded with CH_3COOH or CF_3COOH and without the addition of these complexes, showing a lower measurable current at potentials associated with hydrogen evolution (Fig. S28 and S29, ESI†). A series of CVs were obtained with complexes **1**, **2** and **3** in DMF with acid as the substrate to confirm the HER activity. Then, the glassy carbon working electrode was withdrawn from the solution and washed thoroughly with deionized water, but it was not polished. It is pertinent to mention that upon immersion of this electrode into a fresh set of acid solution and electrolyte, no catalytic current was observed on sweeping the potential in the cathodic region. This fact shows that the HER activity is neither due to the film of catalyst compound nor due to its degraded product,

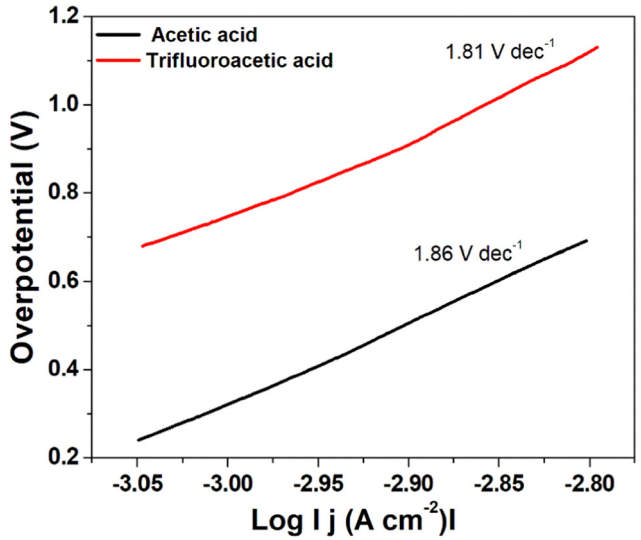

Fig. 8 Tafel plot for hydrogen evolution catalysed by complex **1** using trifluoroacetic acid (red line) and acetic acid (black line) as the acid source.

which could be strongly adsorbed onto the electrode surface. As shown in Fig. S30 (ESI†), the electrolysis did not show appearance of any new bands. These results indicate that complex **1** is stable during electrocatalysis for hydrogen production.

Computational analysis of catalysts and intermediates by DFT-D4. All the complexes were initially optimized by DFT-D4 analysis with def2-TZVP for metal center and def2-SVP for other atoms with the solvent model COSMO (water) and B3LYP.[41] The comparison of the bond length between the geometry optimized structure and X-ray analysis data has been tabulated in ESI† (Table S8). Theoretically calculated UV-vis spectra of complexes **1** and **2** are displayed in ESI† (Fig. S31).

Mechanistic pathways are reportedly known in the literature, based on different reports we propose the plausible mechanism, as depicted in Fig. S32a (ESI†). The pristine catalyst with the Ni(II) center reduced first to Ni(I), which then undergoes oxidative protonation to form a hydride complex {Ni(III)–H} (Tables S9–S20 for geometry optimized coordinates and summary of natural population analysis for complexes and intermediates, ESI†). As per the report of Cao *et al.*,[42] this Ni(III)–H hydride complex either reacts with a proton to produce H_2 and Ni(III) complex (heterolytic route), or is further reduced to Ni(II)–H. This Ni(II)–H can react with a proton to give Ni(II) and H_2, or react with another Ni(II)–H to produce H_2 and 2 molecules of Ni(I) complex. Another way is that Ni(III)–H underwent bimolecular hydrolysis to produce H_2 and the original starting Ni(II) complex. It can be concluded that once the hydride complex is formed, it can liberate hydrogen, and by simultaneous reduction, it gets back to the initial catalyst to continue the cycle.[42,43] This suggests that the key intermediate is Ni(III)–H complexes in a mechanistic cycle of HER. In this work, we wanted to model those complexes and understand their geometries, which, on the one hand, helps to understand the present outcome and, on the other hand, can suggest better geometries for future development. Therefore, we took aid of DFT calculation that helps to understand an interesting trend in dipole moment (Table S21, ESI†), where the highest value was obtained for complex **1**. Indeed, we hypothesize that one reason of showing better catalytic activity for complex **1** can be associated with a higher dipole moment that possibly helps in forming the hydride complex leading to catalysis.[42–44] To understand the geometry of the hydride intermediates, it was calculated at the level of B3LYP + COSMO(H_2O) + def2TZVP(Ni) + def2-SVP(C,H,N,O) which reveals a distorted penta-coordination network for the Ni(III) centre in the complexes. Metal centres of catalysts (complexes **1**, **2** and **3**) comprise the HOMO density, whereas for hydride complexes the metal centres in LUMO comprise the density as obtained from the examined frontier molecular orbitals (Fig. S32b–d and ESI† for population analysis). Thus, from DFT calculations, we understood that shorter aliphatic substitution gives a higher dipole moment that could have an influence on higher catalytic activity. Another aspect that originates from the DFT calculation regarding future development is to keep an aromatic group at the end of the aliphatic chain for aromatic interaction with adjacent aromatic groups for complex **2**. As we observed for complex **2** and its hydride derivative, the aliphatic group is finally inclined towards the aromatic groups. However, for complexes **1** and **3**, such observation was not seen. This possibly suggests an optimum chain length for inclination, and here substitution with an aromatic group could give higher stability of the complex, eventually better catalytic activity.

Conclusions

In summary, we have successfully synthesized three mononuclear nickel(II) complexes with similar N and O donor ligands and characterized them by various standard methods. These complexes have been found to be active electrocatalysts for hydrogen evolution reactions using acetic acid and trifluoroacetic acid as the substrates in DMF. The TOF values of these catalysts decrease with the increase in the chain length of the hydroxyalkyl group. The Ni(II) centre in these complexes is reduced to Ni(I) species and then converted into Ni(III)-hydride, which ultimately generates hydrogen and returns to the Ni(II) state. This possible mechanism has been supported by theoretical calculations. Thus, in this study, it has been demonstrated that the length of the alkyl side chain has significant effects on the catalytic ability in HERs and can be judiciously designed to get optimized efficiency.

Author contributions

Arpita Barma: conceptualization, formal analysis, investigation, methodology; Malay Chakraborty: formal analysis, investigation; Swapan Kumar Bhattacharya: formal analysis, supervision, validation, writing – original draft; Pritam Ghosh: methodology, software, validation, writing – original draft; Partha Roy: conceptualization, resources, supervision, validation, writing – review & editing.

Conflicts of interest

There are no conflicts to declare.

Acknowledgements

AB wishes to thank CSIR, New Delhi for providing her a fellowship.

References

1 J.-W. Wang, W.-J. Liu, D.-C. Zhong and T.-B. Lu, *Coord. Chem. Rev.*, 2019, **378**, 237–261.
2 (*a*) M. G. Pfeffer, T. Kowacs, M. Wächtler, J. Guthmuller, B. Dietzek, J. G. Vos and S. Rau, *Angew. Chem., Int. Ed.*, 2015, **54**, 6627–6631; (*b*) H. Ozawa, M.-A. Haga and K. Sakai, *J. Am. Chem. Soc.*, 2006, **128**, 4926–4927; (*c*) D. Liu, X. Li, S. Chen, H. Yan, C. Wang, C. Wu, Y. A. Haleem, S. Duan, J. Lu, B. Ge, P. M. Ajayan, Y. Luo, J. Jiang and L. Song, *Nat. Energy*, 2019, **4**, 512–518; (*d*) K. Zeng and D. K. Zhang, *Prog. Energy Combust. Sci.*, 2010, **36**, 307–326; (*e*) A. Lasia, Hydrogen evolution reaction, In*Handbook of Fuel Cells*, John Wiley & Sons, New York, 2010; (*f*) J. K. Nørskov, T. Bligaard, A. Logadottir, J. R. Kitchin, J. G. Chen, S. Pandelov and U. Stimming, *J. Electrochem. Soc.*, 2005, **152**, J23–J26; (*g*) J. Greeley, T. F. Jaramillo, J. Bonde, I. Chorkendorff and J. K. Nørskov, *Nat. Mater.*, 2006, **5**, 909–913.
3 (*a*) K. E. Dalle, J. Warnan, J. J. Leung, B. Reuillard, I. S. Karmel and E. Reisner, *Chem. Rev.*, 2019, **119**, 2752–2875; (*b*) L. Tong, L. Duan, A. Zhou and R. P. Thummel, *Coord. Chem. Rev.*, 2020, **402**, 213079.
4 T. Agarwal and S. Kaur-Ghumaan, *Coord. Chem. Rev.*, 2019, **39**, 88–219.
5 M. D. Sampson and C. P. Kubiak, *Inorg. Chem.*, 2015, **54**, 6674–6676.
6 (*a*) A. Z. Haddad, S. P. Cronin, M. S. Mashuta, R. M. Buchanan and C. A. Grapperhaus, *Inorg. Chem.*, 2017, **56**, 11254–11265; (*b*) P. Zhang, M. Wang, Y. Yang, T. Yao and L. Sun, *Angew. Chem., Int. Ed.*, 2014, **53**, 13803–13807.
7 (*a*) N. Queyriaux, D. Sun, J. Fize, J. Pécaut, M. J. Field, M. Chavarot-Kerlidou and V. Artero, *J. Am. Chem. Soc.*, 2020, **142**, 274–282; (*b*) T. Straistari, R. Hardré, J. Fize, S. Shova, M. Giorgi, M. Réglier, V. Artero and M. Orio, *Chem. Eur. J.*, 2018, **24**, 8779–8786; (*c*) N. Kaeffer, M. Chavarot-Kerlidou and V. Artero, *Acc. Chem. Res.*, 2015, **48**, 1286–1295.
8 (*a*) T. Fogeron, T. K. Todorova, J.-P. Porcher, M. Gomez-Mingot, L.-M. Chamoreau, C. Mellot-Draznieks, Y. Li and M. Fontecave, *Dalton Trans.*, 2019, **48**, 14653–14661; (*b*) Y.-P. Zhang, M. Zhang, X.-R. Chen, C. Lu, D. J. Young, Z.-G. Ren and J.-P. Lang, *Inorg. Chem.*, 2020, **59**, 1038–1045; (*c*) R. Shen, J. Xie, Q. Xiang, X. Chen, J. Jiang and X. Li, *Chin. J. Catal.*, 2019, **40**, 240–288; (*d*) D. Jana, H. K. Kolli, S. Sabnam and S. K. Das, *Chem. Commun.*, 2021, **57**, 9910–9913; (*e*) S. Sinha, G. N. Tran, H. Na and L. M. Mirica, *Chem. Commun.*, 2022, **58**, 1143–1146; (*f*) A. Cabrera-García, V. Blay, R. Blay-Roger, Á. G. Ravelo, J. González-Platas, M. C. Arévalo, J. Sanchiz and P. Martín-Zarza, *Chem. Eng. J.*, 2021, **420**, 130342.
9 (*a*) P. Bhanja, B. Mohanty, S. Chongdar, A. Bhaumik, B. K. Jena and S. Basu, *ACS Appl. Energy Mater.*, 2022, **5**, 3558–3567; (*b*) S. Bhattacharjee, S. Bera, R. Das, D. Chakraborty, A. Basu, P. Banerjee, S. Ghosh and A. Bhaumik, *ACS Appl. Mater. Interfaces*, 2022, **14**, 20907–20918; (*c*) H. Xu, H. Shang, C. Wang and Y. Du, *Coord. Chem. Rev.*, 2020, **418**, 213374; (*d*) J. Mohammed-Ibrahim and X. Sun, *J. Energy Chem.*, 2019, **34**, 111–160.
10 R. M. Bullock, A. M. Appel and M. L. Helm, *Chem. Commun.*, 2014, **50**, 3125–3143.
11 J. W. Morgan and E. Anders, *Proc. Natl. Acad. Sci. U. S. A.*, 1980, **77**, 6973–6977.
12 J. Fesseler, J.-H. Jeoung and H. Dobbek, *Angew. Chem., Int. Ed.*, 2015, **54**, 8560–8564.
13 B. J. Fisher and R. Eisenberg, *J. Am. Chem. Soc.*, 1980, **102**, 7361–7363.
14 A. Zarkadoulas, M. J. Field, C. Papatriantafyllopoulou, J. Fize, V. Artero and C. A. Mitsopoulou, *Inorg. Chem.*, 2016, **55**, 432–444.
15 M. L. Helm, M. P. Stewart, R. M. Bullock, M. R. DuBois and D. L. DuBois, *Science*, 2011, **333**, 863–866.
16 G. Bergamini and M. Natali, *Dalton Trans.*, 2019, **48**, 14653–14661.
17 A. Das, Z. Han, W. W. Brennessel, P. L. Holland and R. Eisenberg, *ACS Catal.*, 2015, **5**, 1397–1406.
18 H. Shao, S. K. Muduli, P. D. Tran and H. S. Soo, *Chem. Commun.*, 2016, **52**, 2948–2951.
19 X. Li, Ho, H. Shao, Y. Y. Ng, R. Ganguly, Y. Lu and H. S. Soo, *Inorg. Chem.*, 2019, **58**, 1469–1480.
20 *APEX-II, SAINT and SADABS*, Bruker AXS Inc., Madison, WI, 2008.
21 G. M. Sheldrick, *Acta Crystallogr.*, 2015, **A71**, 3–8.
22 G. M. Sheldrick, *Acta Crystallogr.*, 2015, **C71**, 3–8.
23 L. Yang, D. R. Powell and R. P. Houser, *Dalton Trans.*, 2007, 955–964.
24 (*a*) S. Halder, J. Mondal, J. Ortega-Castro, A. Frontera and P. Roy, *Dalton Trans.*, 2017, **46**, 1943–1950; (*b*) A. Bhattacharjee, S. Dey and P. Roy, *Inorg. Chim. Acta*, 2019, **490**, 93–103.
25 D. L. Pavia, G. M. Lampman, G. S. Kriz and J. R. Vyvyan, *Introduction to spectroscopy*, Cengage Learning, Stamford, USA, 5th edn, 2015.
26 (*a*) M. F. Mehrjardi, H. Kargar, R. B.-Ardakani, M. Ashfaqc, K. S. Munawar and M. N. Tahir, *J. Mol. Struct.*, 2022, **1251**, 132037; (*b*) G. R. Reddy, S. Balasubramanian and K. Chennakesavulu, *J. Mater. Chem. A*, 2014, **2**, 15598–15610; (*c*) A. D. Khalaji, M. Nikookar and D. Das, *J. Therm. Anal. Calorim.*, 2014, **115**, 409–417; (*d*) S. N. Shukla, P. Gaur, M. L. Raidas and B. Chaurasia, *J. Mol. Struct.*, 2020, **1202**, 127362; (*e*) H. Kargr, A. A. Ardakani, M. N. Tahir, M. Ashfaqc and K. S. Munawar, *J. Mol. Struct.*, 2021, 129842.
27 (*a*) S. Chattopadhyay, M. S. Ray, S. Chaudhuri, G. Mukhopadhyay, G. Bocelli, A. Cantoni and A. Ghosh,

Inorg. Chem. Acta, 2006, **359**, 1367–1375; (*b*) M. S. Ray, S. Chaudhuri, L. Right, G. Bocelli, G. Mukhopadhyay and A. Ghosh, *Polyhedron*, 2003, **22**, 617–624.

28 (*a*) B. S. Garg and D. N. Kumar, *Spectrochim. Acta, Part A*, 2003, **59**, 229–234; (*b*) A. Anthonysamy and S. Balasubramanian, *Inorg. Chem. Commun.*, 2005, **8**, 908–911.

29 (*a*) M. Salehi, F. Rahimifar, M. Kubicki and A. Asadi, *Inorg. Chim. Acta*, 2016, **443**, 28–35; (*b*) A. Barma, D. Ghosh, P. Karmakar and P. Roy, *J. Mol. Struct.*, 2022, **1250**, 131687.

30 A. Ourari, Y. Ouennoughi, D. Aggoun, M. S. Mubarak, E. M. Pasciak and D. G. Peters, *Polyhedron*, 2014, **67**, 59–64.

31 L.-Q. Chai, H.-S. Zhang, J.-J. Huang and Y.-L. Zhang, *Spectrochim. Acta, Part A*, 2015, **137**, 661–669.

32 J. Datta, S. Bhattacharya and K. K. Kundu, *Aust. J. Chem.*, 1983, **36**, 1779–1784.

33 C. Chen, X. Li, F. Deng and J. Li, *RSC Adv.*, 2016, **6**, 79894–79899.

34 T. D. Cook, S. F. Tyler, C. M. McGuire, M. Zeller, P. E. Fanwick, D. H. Evans, D. G. Peters and T. Ren, *ACS Omega*, 2017, **2**, 3966–3976.

35 V. Fourmond, P.-A. Jacques, M. Fontecave and V. Artero, *Inorg. Chem.*, 2010, **49**, 10338–10347.

36 (*a*) V. Fourmond, S. Canaguier, B. Golly, M. J. Field, M. Fontecave and V. Artero, *Energy Environ. Sci.*, 2011, **4**, 2417–2427; (*b*) G. A. N. Felton, R. S. Glass, D. L. Lichtenberger and D. H. Evans, *Inorg. Chem.*, 2006, **45**, 9181–9184.

37 (*a*) J.-P. Cao, T. Fang, L.-Z. Fu, L.-L. Zhou and S. Zhan, *Int. J. Hydrogen Energy*, 2014, **39**, 10980–10986; (*b*) R. Jain, A. A. Mamun, R. M. Buchanan, P. M. Kozlowski and C. A. Grapperhaus, *Inorg. Chem.*, 2018, **57**, 13486–13493; (*c*) G. Bergamini and M. Natali, *Dalton Trans.*, 2019, **48**, 14653–14661; (*d*) Y.-P. Zhang, M. Zhang, X.-R. Chen, C. Lu, D. J. Young, Z.-G. Ren and J.-P. Lang, *Inorg. Chem.*, 2020, **59**, 1038–1045; (*e*) J.-M. Lei, S.-P. Luo and S.-Z. Zhan, *Int. J. Hydrogen Energy*, 2018, **43**, 19047–19056; (*f*) Q.-X. Peng, D. Xue, S.-Z. Zhan and C.-L. Ni, *Appl. Catal. B*, 2017, **219**, 353–361; (*g*) L. Chen, G. Chen, C.-F. Leung, S.-M. Yiu, C.-C. Ko, E. A. Mallart, M. Robert and T.-C. Lau, *ACS Catal.*, 2015, **5**, 356–364.

38 (*a*) C. Costentin, S. Drouet, M. Robert and J.-M. Saveant, *J. Am. Chem. Soc.*, 2012, **134**, 11235–11242; (*b*) C. Costentin, M. Robert and J.-M. Saveant, *Chem. Soc. Rev.*, 2013, **42**, 2423–2436; (*c*) C. Costentin and J.-M. Saveant, *ChemElectroChem*, 2014, **1**, 1226–1236; (*d*) R. J. DiRisio, J. E. Armstrong, M. A. Frank, W. R. Lake and W. R. McNamara, *Dalton Trans.*, 2017, **46**, 10418–10425.

39 N. Elgrishi, M. B. Chambers and M. Fontecave, *Chem. Sci.*, 2015, **6**, 2522–2531.

40 (*a*) V. S. Thoi, Y. Sun, J. R. Long and C. J. Chang, *Chem. Soc. Rev.*, 2013, **42**, 2388–2400; (*b*) M. Zeng and Y. Li, *J. Mater. Chem. A*, 2015, **3**, 14942–14962; (*c*) X. Zou and Y. Zhang, *Chem. Soc. Rev.*, 2015, **44**, 5148–5180.

41 (*a*) *TURBOMOLE, Version 7.3, a development*, University of Karlsruhe and Forschungszentrum Karlsruhe GmbH, 1989–2007; (*b*) E. Caldeweyher, C. Bannwarth and S. Grimme, *J. Chem. Phys.*, 2017, **147**, 034112.

42 Y. Han, H. Fang, H. Jing, H. Sun, H. Lei, W. Lai and R. Cao, *Angew. Chem., Int. Ed.*, 2016, **55**, 5457–5462.

43 K. Majee, J. Patel, S. Rai, B. Das, B. Panda and S. K. Padhi, *Phys. Chem. Chem. Phys.*, 2016, **18**, 21640–21650.

44 N. Villegas-Escobar, D. E. Ortega, D. Cortes-Arriagada, R. Duran, D. Yepes, S. Gutierrez-Oliva and A. Toro-Labbe, *J. Phys. Chem. C*, 2017, **121**, 12127–12135.